Available online at www.sciencedirect.com
SCIENCE DIRECT®
Journal of Solid State Chemistry 177 (2004) 1631–1638
JOURNAL OF SOLID STATE CHEMISTRY
http://elsevier.com/locate/jssc

Pressure–temperature phase diagram of SeO_2. Characterization of new phases

D. Orosel, O. Leynaud, P. Balog, and M. Jansen*

Max-Planck Institute for Solid State Research, Heisenbergstrasse 1, D-70569 Stuttgart, Germany

Received 26 September 2003; received in revised form 24 November 2003; accepted 14 December 2003

Abstract

We have investigated SeO_2 at high pressures and high temperatures. Two new phases (β-SeO_2 and γ-SeO_2) and the boundary separating them have been found, following experimental runs performed at pressures up to 15 GPa and temperatures up to 820°C. The two phases crystallize in the orthorhombic system in space group $Pmc2_1$ (no. 26) with $a = 5.0722(1)$ Å, $b = 4.4704(1)$ Å, $c = 7.5309(2)$ Å, $V = 170.760(9)$ Å^3 and $Z = 4$ for the β-phase, and with $a = 5.0710(2)$ Å, $b = 4.4832(2)$ Å, $c = 14.9672(6)$ Å, $V = 340.27(3)$ Å^3 and $Z = 8$ for the γ-phase. Both phases are stable at ambient pressure and temperature below −30°C. At ambient temperature the phases return to the starting phase (α-SeO_2) in a few days. We discuss our findings in relation to a previous report of in-situ measurements at high pressures and ambient temperature.

Keywords: SeO_2; New phase; High pressure and high temperature

1. Introduction

The role of lone electron pairs in structural chemistry was pointed out 30 years ago [1,2], and in-detail discussions on the geometry of coordination polyhedra including lone pairs were presented later [3]. More precisely, this latter study is attributing an occupied volume for the lone pair which is considered to be equivalent to the volume commonly filled by an oxygen atom. The importance of the lone pair compounds has increased progressively with the interesting structural properties arising for these compounds, especially due to the usually very pronounced stereoactivity of the lone pair. Moreover, the almost systematic orientation of the lone pairs along certain directions can act as a starting point of building open frameworks, since lone pairs tend to point together towards the center of a cavity [4–7], or inside an interplanar space, giving rise to lamellar compounds [8–10].

The lone electron pairs are also responsible for various physical properties. For example, as a consequence of the strong anisotropy of the environment (all the bonds between anions and the lone pair element being packed on one side, with the lone pair occupying the other side) the materials are generally exhibiting high polarizability [11], which can give rise to physical properties such as ferroelectricity or piezoelectricity [12,13].

The lone pairs are susceptible to play a role in temperature-induced phase transitions [14,15], and in some cases (e.g., Bi and Pb compounds), in pressure-induced phase transitions [16,17]. These transformations are generally difficult to predict due to the various possible responses upon applied external stress. The lone pair–lone pair interaction is generally assumed to stabilize a structure [6,8], but if there is a pressure-induced delocalization of the lone pair, the compound could exhibit "metallic" behavior. Also, even slight changes in the orientation or the alignment of the lone pairs could be associated with a phase transition [12,14]. In addition to the above-mentioned examples of Bi and Pb compounds, pressure-induced phase transitions were also reported for TeO_2 [18] and more recently, for SeO_2 [19].

The goal of the present study of such basic binary systems is to find quenchable high-pressure phases, stable at ambient conditions (similar to Bi_2O_3 [16]), and perhaps exhibiting novel electronic properties. The compound of solid selenium dioxide has only one

*Corresponding author. Fax: +49-711-689-1502.
E-mail address: m.jansen@fkf.mpg.de (M. Jansen).

0022-4596/$ - see front matter © 2004 Elsevier Inc. All rights reserved.
doi:10.1016/j.jssc.2003.12.028

known stable modification (noted α-SeO_2) at ambient pressure and temperatures approaching 300°C [20,21]. SeO_2 crystallizes in the tetragonal space group $P4_2/mbc$ (no. 135) with $a = 8.3622$ Å, $c = 5.0612$ Å, $V = 353.9$ Å^3 and $Z = 8$. Recently, a high-pressure modification of selenium dioxide was reported at pressures above 7 GPa (noted Grz–SeO_2), in in situ XRD in diamond-anvil cell (DAC) experiments at room temperature [19]. This new metastable phase is not pressure-quenchable, and an orthorhombic space group *Pbam* (no. 55) with $a = 8.134$ Å, $b = 7.928$ Å, $c = 4.949$ Å, $V = 319.6$ Å^3 and $Z = 8$ was proposed to describe it. To probe this result, we have performed an experiment at 23°C and 9 GPa, for 52 h, in a large volume press. Post-decompression, only the starting phase was present in the sample, and not even traces of any phase derived from a pressure-induced transformation were observed.

For the next heavier element in group 16 (Te), tellurium dioxide (α-TeO_2), the high-pressure behavior has been also discussed in a review paper [18], but the study suggests that only a second order phase transformation occurs at 0.9 GPa and room temperature. The tetragonal space group $P4_22_12$ (no. 92) of α-TeO_2 with $a = 4.808$ Å, $c = 7.612$ Å, $V = 175.9$ Å^3 and $Z = 4$ changes to an orthorhombic space group $P2_12_12$ (no. 18) with $a = 4.605$ Å, $b = 4.856$ Å, $c = 7.530$ Å, $V = 168.4$ Å^3 and $Z = 4$.

We have performed high-pressure and high-temperature experiments on α-SeO_2, in order to identify novel phases, stable after returning to ambient conditions.

2. Experimental details

The experimental runs have been carried out at pressures up to 15 GPa and temperatures up to 820°C, using a piston-cylinder press and a belt press for the lower pressure range, and a multianvil press for higher pressures. The multianvil press (Voggenreiter GmbH, Germany) employed a Walker module equipped with sets of 32 mm WC cubes of 11 and 8 mm truncation edge length, respectively. The press was previously calibrated in pressure at room and elevated temperature. Graphite and $LaCrO_3$ cylindrical heaters were used for obtaining high temperatures through Joule effect in the high-pressure cells. Temperature was measured using thermocouples placed in close vicinity to the sample containers. The starting material was white crystalline powder of SeO_2 (99.999% Sigma-Aldrich). This was dried at 150°C for 4 days under a flow of dry oxygen. After drying, the selenium dioxide was handled and stored in a glove box flooded with dry argon. For the experiments, SeO_2 was packed in tightly closed Pt crucibles, in order to avoid contamination. The filled crucibles were placed in the press and then kept at pressures between 2 and 15 GPa and temperatures up to 820°C for 15–24 h. Afterwards, the experiments were temperature-quenched, while pressure was released at a slow rate, in order to avoid blow-outs and anvil damage.

Post-experiment, the samples were opened in the glove box. The absence of water was controlled by infrared spectroscopy. The two new selenium dioxide phases are white powders. Because no single crystal of sufficient size could be found, the structures were solved from powder diffraction data. Due to the fact that the high pressure phases are metastable at room temperature, the X-ray pattern were collected on a STOE Stadi P with Cu$K\alpha$1 and with an attached Oxford Cryo cooling device. During the measurement, the capillaries with the powder samples were kept at 200 K. At this temperature no back transformation to the ambient pressure phase could be detected. Indexing of the new modifications of β-SeO_2 and γ-SeO_2 was done with the software CRYSFIRE [22]. The structures were solved by "ab initio" methods with ENDEAVOUR [23,24,25], and the final refinements were done with GSAS [26]. Density measurements were done with an AccuPyc 1330 GB (Micromeritics, Germany). For Raman spectra of the new phases, powders were sealed in quartz capillaries and measured with a LabRAM System from Jobin-Yvon, Horiba. The Raman scattering was excited at a laser wavelength of 632.8 nm and a laser power of 0.4 mW. The infrared data of the starting material and the sample were collected by preparation of KBr pellets, which were measured on a FT-IR-Spektrometer IFS-113v (Bruker, Germany).

3. Experimental results

3.1. High-pressure and high-temperature phases

The results of the high pressure (up to 15 GPa) and high temperature (up to 820°C) runs are shown in Fig. 1.

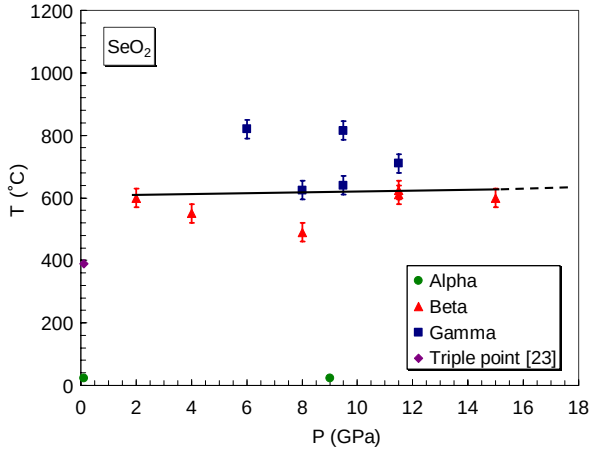

Fig. 1. *P–T* phase diagram for SeO_2. The boundary between α and β phases was not investigated.

The symbols shown correspond to the detected phases, post-quenching and slow pressure release. Two new (metastable) high-pressure modifications of SeO_2 were found, noted β-SeO_2 and γ-SeO_2, respectively. The continuous line separating the two phases is well constrained, and could be considered, within the associated error bars, to be the phase boundary between the two new phases. The attached error bars correspond to the combined uncertainty in temperature measurement and a small temperature gradient in the high-pressure cell. Fig. 1 also contains the literature reported [23] triple point of SeO_2, 389.3°C at approximately 9 bars. The integrity of the two new phases is perfectly maintained at room pressure and temperature below −30°C. Long time exposure (days) to ambient temperatures triggers the return to the starting α-SeO_2 phase.

3.2. Structure refinement of β-SeO_2 and γ-SeO_2

The X-ray diffraction patterns of β-SeO_2 and γ-SeO_2 can be explained neither with the parameters of the room temperature and pressure compound α-SeO_2 [21], nor with those proposed in previous studies at high pressure and room temperature [19]. In order to solve these new structures for the SeO_2 compounds, reflections were indexed with the help of the CRYSFIRE software [22], and after checking systematic extinctions for both β- and γ-SeO_2, three space groups were found possible, *Pma*2 (no. 28), *Pmma* (no. 51) and *Pmc*2_1 (no. 26). Only the latter gives, with the help of the "ab initio" software ENDEAVOUR [23,24,25], a reasonable solution for the atomic positions for each of both phases. These sets of data were used for the refinements with the GSAS software [26]. The parameters refined are the scale factor, the background, the lattice parameters, the profile using a pseudo-Voigt function, the atomic positions, and the isotropic thermal parameters. The z position being free in this space group, the value of zero was arbitrary set as the z position of one of the Se atoms. The refined X-ray patterns are shown in Fig. 2 (a and b) for β-SeO_2 and γ-SeO_2, and no noticeable broadening, as previously reported for Grz–SeO_2 [19], is observable (the introduction of such phenomena into the refinements was tried, with no real improvement). Finally, due to high X-ray absorption of these compounds, an absorption correction was applied. The refined cell parameters and the refinement conditions are given in Table 1. The final refined atomic positions and distances are displayed in Tables 2 and 3.

3.3. Structural description

The compounds are all formed by simple SeO_3E entities (E represents the lone pair), built on the basis of a trigonal pyramid. The Se atom placed in the center, is surrounded at its basis by three oxygen atoms, and on the apex by the lone pair. Due to symmetry breaking, two distinct SeO_3E entities are present in β-SeO_2, four are observable in γ-SeO_2, while only one seems to exist in α-SeO_2. The spatial arrangement of these building blocks inside the cell is constructed on a 1-D configuration present inside all the phases. Strings are formed by a zigzag succession of corner-shared basic pyramidal entities. The two non-shared corners are occupied by one "double-bonded" oxygen atom, and by the lone pair. The particularity of this string is that all the lone pairs are oriented in the same direction. Another simple method to describe these phases is shown on Fig. 3, where only the projections, of the rows of atoms in the plane perpendicular to the string direction, are represented. The W-shapes are oriented with the central O-atom bonding the two selenium atoms along the string direction. The two other atoms (one on each side of the string) are the "double-bonded" oxygen atoms.

With the exception of Grz–SeO_2, where the structure is similar to α-SeO_2, with very strong deformations of the local building blocks, the main difference between the SeO_2 phases is in the arrangement and orientation of these W-shapes. As shown in Fig. 3, various orientations of the predefined W-shape are possible. For α-SeO_2 (Fig. 3a) the arrangement of four entities (in a projection in the plane perpendicular to the string) gathered around one 4-fold axis generates four orientations in the plane for the W-shape. The β-SeO_2 structure is definitely different with its only two different orientations for the W-shape (Fig. 3b), which are stacked by alternate "planes" of each orientation. Finally, γ-SeO_2 contains the same two orientations for the W-shape, similar to β-SeO_2, but in this case the "planes" are stacked by pairs of alternate "planes" (Fig. 3c), leading to the doubling of the cell along the stacking axis.

It may be interesting to point out the inter-chain distances between the selenium atoms and the oxygen atoms of two neighboring strings. These values, about 2.7 to 3.0 Å (see Table 3), are shorter than those expected for a Van der Waals bond, implying that these bonds could be playing a role in the stability of the phases.

3.4. Lattice energy calculations

The motives of mutual allocation, the effective coordination number ECON and the mean fictive ionic radii MEFIR [29] have been calculated and are listed in Table 4. For β-SeO_2 and γ-SeO_2 the values are in good agreement for the same type of ions and they are in the expected range. This is an indication of well-balanced crystal structures for the new high pressure and high temperature phases of SeO_2. The values for the Madelung part of the lattice energy [30] are for identical ions of the same magnitude and are shown in Table 5. The Coulomb part of the lattice energy for β-SeO_2 (13,035 kJ/mol) is similar to that of α-SeO_2 (13,029 kJ/mol). For the γ-SeO_2

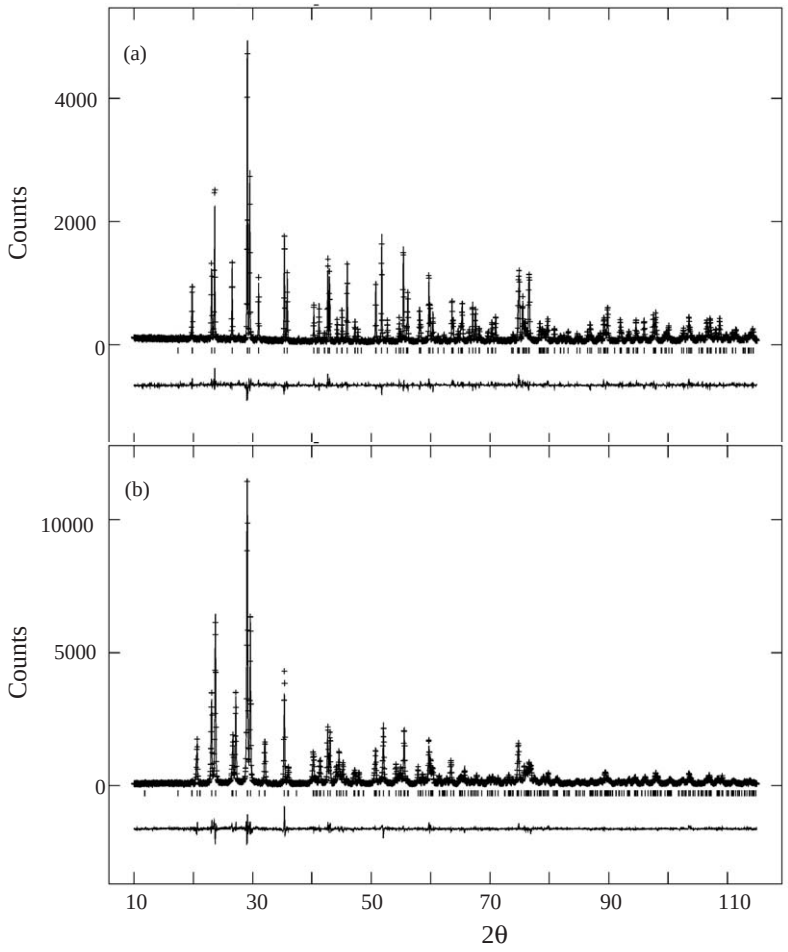

Fig. 2. X-ray diffraction patterns of β-SeO_2 (a) and γ-SeO_2 (b). Crosses (+) are the experimental data, the line is the calculated pattern. The difference is plotted under the bars which are representing the positions of the Bragg diffraction peaks.

Table 1
Crystallographic and least-square refinement data for β-SeO_2 and γ-SeO_2

Crystallographic data[a]	β-SeO_2	γ-SeO_2
a (Å)	5.0722(1)	5.0710(2)
b (Å)	4.4704(1)	4.4832(2)
c (Å)	7.5309(2)	14.9672(6)
V (Å^3)	170.760(9)	340.27(3)
Space group	$Pmc2_1$ (no. 26)	
Z	4	8
Calculated unit cell formula weight	443.832	887.664
D_{calc}/D_{meas}	4.316/4.3(1)	4.332/[b]
Temperature (K)	200	
Least-square refinement data (%)[c]		
wR_p	10.54	13.72
R_p	8.11	9.55
Reduced χ^2	1.73	4.82
$R(F^2)$	7.32	5.02

[a] Estimated standard deviations (e.s.d.) values were multiplied by 3 in order to take in account local correlations as described by Bérar [27].
[b] Could not be determined due to reduced sample size.
[c] As given in the GSAS manual.

Table 2
Atomic positions and thermal parameters of the phases β-SeO_2 and γ-SeO_2

Atom	Site	x	y	z	B_{iso} (Å^2)[a]
β-SeO_2					
Se1	2b	1/2	0.2516(6)	0[b]	0.78(5)
Se2	2a	0	0.1219(6)	0.3748(5)	0.73(5)
O1	2a	0	0.746(4)	0.672(2)	0.8(3)
O2	4c	0.247(2)	0.152(2)	0.841(1)	1.0(2)
O3	2b	1/2	0.620(3)	−0.039(2)	0.9(3)
γ-SeO_2					
Se1	2b	1/2	0.027(1)	0[b]	1.5(2)
Se2	2b	1/2	0.511(2)	0.2492(12)	1.4(2)
Se3	2a	0	0.107(2)	0.6894(7)	1.2(2)
Se4	2a	0	0.344(2)	0.4369(7)	1.4(2)
O1	2a	0	0.476(8)	0.337(4)	2.8(1.4)
O2	2a	0	0.027(6)	0.090(3)	0.1(9)
O3	2b	1/2	0.617(8)	0.486(3)	3.0(1.1)
O4	2b	1/2	0.166(8)	0.225(3)	1.3(9)
O5	4c	0.254(6)	0.624(6)	0.176(2)	2.2(9)
O6	4c	0.248(5)	0.061(2)	0.419(2)	0.6(6)

[a] $B_{iso} = 8\pi^2 . U_{iso}$.
[b] Value of z was arbitrarily set to zero for Se1 due to free axis along c.

Table 3
Distances and angles for the compounds SeO_2[a]

	Distances (Å)											
	α-SeO_2[b]			β-SeO_2			γ-SeO_2			Grz–SeO_2[c]		
Within chains												
Se–$O_{bridged}$[d]	Se–O2	(2x)	1.795(1)	Se1–O2	(2x)	1.81(1)	Se2–O5	(2x)	1.75(3)	Se1–O1	(2x)	1.91(1)
				Se2–O2	(2x)	1.77(1)	Se3–O5	(2x)	1.77(3)	Se2–O1	(2x)	1.77(1)
							Se1–O6	(2x)	1.80(3)			
							Se4–O6	(2x)	1.81(3)			
Se–O_{apical}[e]	Se–O1		1.624(2)	Se1–O3		1.67(2)	Se2–O4		1.58(4)	Se1–O2		1.72(2)
				Se2–O1		1.64(2)	Se3–O2		1.59(5)	Se2–O3		1.49(2)
							Se1–O3		1.60(3)			
							Se4–O1		1.60(6)			
Between chains												
	Se–O1	(2x)	2.843(1)	Se1–O1	(2x)	2.85(1)	Se2–O1	(2x)	2.86(3)	Se1–O3	(2x)	2.85
	Se–O2		2.743(2)	Se1–O3		2.84(2)	Se2–O4		2.97(3)	Se1–O2		2.66(2)
				Se2–O1		2.80(2)	Se3–O1		2.90(5)	Se2–O3		2.57(2)
				Se2–O3	(2x)	2.86(1)	Se3–O4	(2x)	2.87(2)	Se2–O2	(2x)	2.78
							Se1–O2	(2x)	2.87(2)			
							Se1–O3		2.90(3)			
							Se4–O2		2.83(4)			
							Se4–O3	(2x)	2.91(2)			
	Angles (deg.)											
α-SeO_2				β-SeO_2			γ-SeO_2			Grz–SeO_2		
O2–Se1–O2		89.48(5)		O2–Se1–O3	(2x)	97.3(5)	O4–Se2–O5	(2x)	98.1(4)	O1–Se1–O2	(2x)	116.2
O2–Se1–O3	(2x)	98.41(7)		O2–Se1–O2		90.3(7)	O5–Se2–O5		91.7(7)	O1–Se1–O1		71.4
				O2–Se2–O2		90.3(6)	O5–Se3–O5		93.2(7)	O1–Se2–O1		100.1
				O1–Se2–O2	(2x)	96.7(5)	O2–Se3–O5	(2x)	98.2(4)	O1–Se2–O3	(2x)	79.9
							O3–Se1–O6	(2x)	97.3(5)			
							O6–Se1–O6		90.1(6)			
							O6–Se4–O6		88.5(6)			
							O1–Se4–O6	(2x)	96.9(4)			
Se–O2–Se		121.26(4)		Se1–O2–Se2		125.3(6)	Se2–O5–Se3		130.4(7)	Se1–O1–Se2		110.4
							Se1–O6–Se4		123.4			

[a] Atoms labels are those given in Refs. [19] and [21]. Data given on a same table line can be directly compared.
[b] Distances and angles are taken from [21].
[c] Distances and angles are taken from [19]. Values without e.s.d. are calculated on the basis of crystallographic data with the software Diamond [28].
[d] Se–$O_{bridged}$ correspond to distances between a selenium atom to an oxygen connecting another selenium atom.
[e] Se–O_{apical} correspond to distances between a selenium atom and a "double-bond"oxygen atom.

phase the Coulomb part of the lattice energy is just slightly higher (13,208 kJ/mol). For Grz–SeO_2 phase there is a significant difference in the values of ECON and MEFIR for identical ions (Table 4). This applies for the Madelung and Coulomb parts of the lattice energy as well. Such results suggest a poorly balanced crystal structure of Grz–SeO_2, and provide a potential explanation of the completely reversible transformation of the high-pressure phase back to the α-SeO_2 upon decompression. We conclude therefore, that the proposed Grz–SeO_2 phase is unbalanced, and likely to be inaccurate.

3.5. Raman spectroscopy

In the Raman spectra of β-SeO_2 and γ-SeO_2 (Fig. 4) some bands are shifted and broadened due to the high pressure and some new bands appear. The new Raman peaks could result from the lifted degeneracy of the E_g modes by the lowering of crystal symmetry of α-SeO_2 $P4_2/mbc$ (D_{4h}^{13}) to crystal symmetry $Pmc2_1$ (C_{2v}^2) of β-SeO_2 and γ-SeO_2, and the splitting of the Se and O positions in the new high-pressure and high-temperature phases. According to Ref. [31], Raman peaks around 900 cm^{-1} can be assigned to Se–O stretches (terminal oxygen atoms). In the 500–750 cm^{-1} range, the peaks correspond to O–Se–O chain stretching modes, including symmetric and asymmetric types. The peaks in the 190–360 cm^{-1} range belong to various O–Se–O bending modes, higher wave numbers involving terminal oxygen atoms. The Raman spectra of β-SeO_2 and γ-SeO_2 exhibit over the whole wave number range nearly the same behavior. In the region between 215 and 340 cm^{-1} the

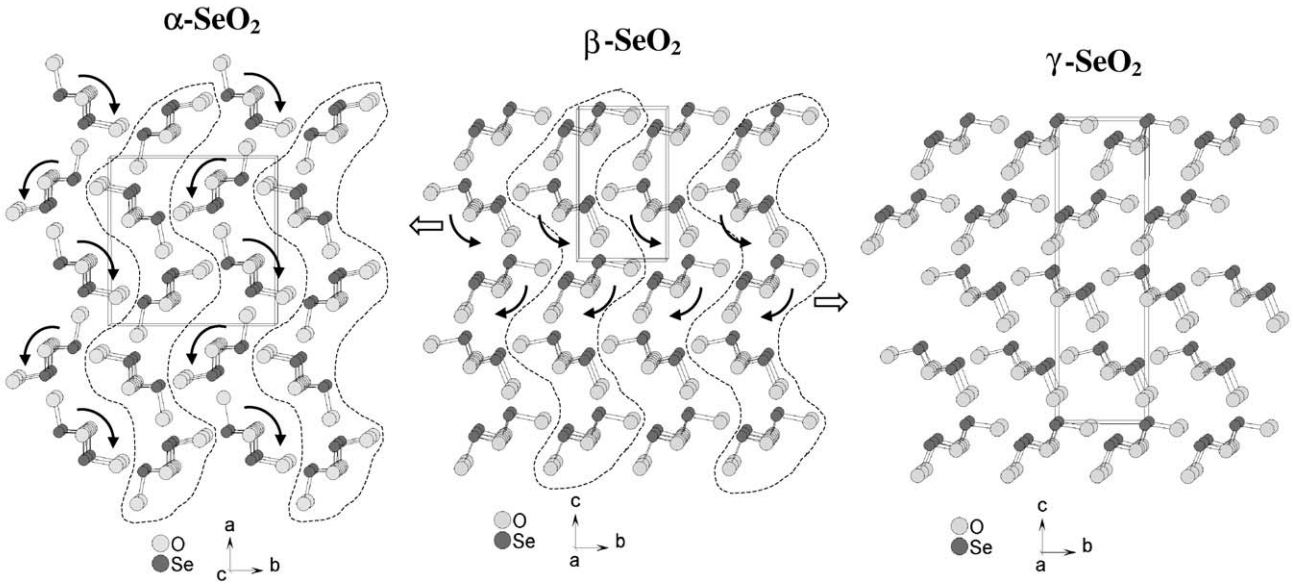

Fig. 3. Projection of the different polymorphic modifications of SeO_2 onto the plane perpendicular to the strings. (a) α-SeO_2; (b) β-SeO_2; (c) γ-SeO_2.

Table 4
Motives of mutual allocation (pm), ECON and MEFIR (pm)

					ECON	MEFIR
α-SeO_2						
	Se					
O1	2/2, 180 (2x)				2.0	155
O2	1/1, 162				1.0	140
ECON	2.8					
MEFIR	24					
β-SeO_2						
	Se1	Se2				
O1	0/0	1/1, 163			1.0	140
O2	2/1, 181 (2x)	2/1, 177 (2x)			2.0	151
O3	1/1, 167	0/0			1.0	140
ECON	2.9	2.9				
MEFIR	29	25				
γ-SeO_2						
	Se1	Se2	Se3	Se4		
O1	0/0	0/0	0/0	1/1, 160	1.0	140
O2	0/0	0/0	1/1, 159	0/0	1.0	140
O3	1/1, 160	0/0	0/0	0/0	1.0	140
O4	0/0	1/1, 158	0/0	0/0	1.0	140
O5	0/0	2/1, 175 (2x)	2/1, 177 (2x)	0/0	2.0	155
O6	2/1, 180 (2x)	0/0	0/0	2/1, 181 (2x)	2.0	158
ECON	2.7	2.8	2.8	2.6		
MEFIR	22	19	21	22		
Grz–SeO_2						
	Se1	Se2				
O1	2/1, 191 (2x)	2/1, 178 (2x)			1.9	160
O2	2/1, 172	0/0			1.0	140
O3	0/0	1/1, 149			1.0	140
ECON	2.6	1.8				
MEFIR	34	9				

Table 5
Madelung part of lattice energy

	Charge	PMF	MAPLE (kJ/mol)
α-SeO_2			
Se	+4	9.55	1951
O1	−2	2.75	561
O2	−2	2.93	599
			$\Sigma = 13024$
β-SeO_2			
Se1	+4	9.63	1954
Se2	+4	9.76	1980
O1	−2	2.76	560
O2	−2	2.91	592
O3	−2	2.69	547
			$\Sigma = 13028$
γ-SeO_2			
Se1	+4	9.41	1975
Se2	+4	9.69	2034
Se3	+4	9.60	2014
Se4	+4	9.30	1952
O1	−2	2.72	570
O2	−2	2.72	571
O3	−2	2.73	573
O4	−2	2.66	558
O5	−2	2.86	599
O6	−2	2.81	587
			$\Sigma = 13208$
Grz–SeO_2			
Se1	+4	8.42	1879
Se2	+4	9.06	2023
O1	−2	2.26	504
O2	−2	2.44	544
O3	−2	2.71	606
			$\Sigma = 12697$

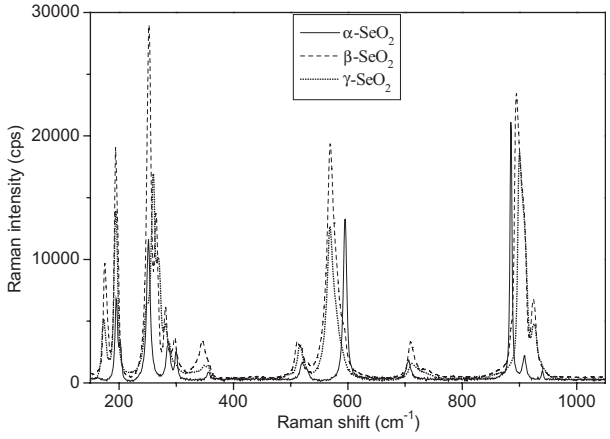

Fig. 4. Raman spectra of α-SeO_2 (full line), β-SeO_2 (dashed line) and γ-SeO_2 (dotted line).

spectra show different peak positions and peak intensities. This can be a result of the two independent SeO_2 chains in γ-SeO_2 instead of one chain in β-SeO_2.

4. Discussion and conclusion

In order to obtain information of the eventual relations between all the phases, the values of the distances and angles of the refined structures should be compared. It is clear that these values are in the same range to those of the starting α-SeO_2 phase. The sum of the O–Se–O angles remains invariable, and only Se–O–Se angles and "double" bonds seem to show slight deformations. This similarity is also true for the second coordination shell, despite of the different arrangement of the strings, which, combined with the results of the lattice energy calculations, provide good arguments for explaining the metastability of the β- and γ-SeO_2 phases at room pressure. In these conditions, β- and γ-SeO_2 are considered quenchable high-pressure phases of SeO_2, the structure being maintained stable below −30°C. Contrarily to these observations, the Grz–SeO_2 phase was not observed at room pressure. This instability can be expressed as a consequence of the very strong electronic unbalance and to the important (and difficult to explain) crystallographic differences between the two different Se atoms. At this point, one should seriously reconsider the validity of the structure proposed for the so-called high-pressure phase Grz–SeO_2 [19]. The reported XRD pattern [19] does not contain any new peaks, and is therefore unlikely to be the result of a new phase. There is no real experimental evidence to support the suggested orthorhombic splitting, and the peak broadening could be just pressure induced. Moreover, the refined value of 1.49 Å is too small even for an Se–O bond at the pressures considered.

Following, we propose a hypothesis for the β- to γ-phase transitions. A more attentive analysis of the arrangement of the β-SeO_2 structure is showing similarities with the α-SeO_2 phase. One "half" of the starting structure is retained, as can be verified in Fig. 3. The succession of the strings and their orientations inside the dashed forms are identical between the model of α-SeO_2 and β-SeO_2. This identification of the remaining parts of the mother structure can be a starting point in the explanation of the origin and the occurrence of the phase transition. It consists of compression in one of the directions of the square plane, leading to an alignment of the planes orthogonal to this direction. The other strings are related to their starting positions by an alternative rotation of $\pm\pi/2$ (roughly) and a translation of $c/2$. The transition to the γ-SeO_2 phase is easier to visualize, with an opposite tilting of two successive "planes" of W-shape entities (rotation close to $\pm\pi/6$). This tilting is combined with opposite translations along b-axis for each "plane" and along c ($c/2$).

The pressure homology rule indicates that the space group of a high-pressure phase should be similar to the space group of the next heavier element in the same group at ambient conditions. For selenium and

tellurium dioxide this rule does not seem applicable. Both oxides show the same transition upon pressure increase, they change from the tetragonal to the orthorhombic crystal system.

We have found two novel high-pressure and high-temperature dimorphic phases for the compound SeO_2, as well as the phase boundary separating the two phases. These phases are quenchable at room pressure, and are stable at temperature below $-30^{\circ}C$. The chains present in the 1 atmosphere pressure phase (α-SeO_2) are maintained, suggesting that the phase transitions observed are due to the chains' movement. What exactly triggers such phase transitions is not yet fully understood.

The high pressure and temperature experiments described above have been performed using three different presses, employing various high-pressure cell geometries and materials. The successful construction of a new, well constrained, phase boundary between the two new phases, is a confirmation of the internal consistency of the simultaneous pressure–temperature approach and of the experimental technique. This seems to be an efficient path for obtaining new stable or (partly) metastable phases, suggesting that the technique should be employed in studying other similar systems.

Further experiments are required, in order to fully determine the combined role which pressure, temperature and kinetics have on the transformations already observed, and to reveal potential structural and electronic modifications in the higher pressure and temperature range.

Acknowledgments

We would like to thank A. Kabutke for preliminary experimental work. We gratefully acknowledge the financial support from Fonds der Deutschen Chemischen Industrie.

References

[1] S. Anderson, A. Åström, Solid State Chem. Proceed of the fifth Materials Research Symposium, NBS Spec. Publ. 364 (1972) 3–14.
[2] S. Anderson, A. Åström, J. Galy, G. Meunier, J. Solid State Chem. 6 (1973) 187–190.
[3] J. Galy, G. Meunier, S. Anderson, A. Åström, J. Solid State Chem. 13 (1975) 142–159.
[4] B. Darriet, J. Galy, Acta Cryst. B 33 (1977) 1489–1492.
[5] M.S. Wickleder, Chem. Rev. 102 (2002) 2011–2087 (and references therein).
[6] P. Millet, L. Sabadié, J. Galy, J.C. Trombe, J. Solid State Chem. 173 (2003) 49–53.
[7] J. Leclaire, J. Chardon, B. Provost, Raveau, J. Solid State Chem. 163 (2002) 308–312.
[8] S. Obbade, M. Huve, E. Suard, M. Drache, P. Conflant, J. Solid State Chem. 168 (2002) 91–99.
[9] M. Johnsson, K.W. Törnroos, Solid State Sci. 5 (2003) 263–266.
[10] J.P. Laval, L. Guillet, B. Frit, Solid State Sci. 4 (2002) 549–556.
[11] V.T. Avanesyan, V.A. Bordovskii, S.A. Potachev, J. Non-Cryst. Solids 305 (2002) 136–139.
[12] L. Nistor, G. Van Tendeloo, S. Amelinckx, V. Kahlenberg, H. Böhm, J. Solid State Chem. 119 (1995) 281–288.
[13] J.C. Champarnaud-Mesjard, S. Blanchandin, P. Thomas, A. Mirgorodsky, T. Merle-Méjean, B. Frit, J. Phys. Chem. Solids 61 (2000) 1499–1507.
[14] J.-M. Kiat, P. Garnier, M. Pinot, J. Solid State Chem. 91 (1991) 339–349.
[15] J.-M. Kiat, P. Garnier, G. Calvarin, M. Pinot, J. Solid State Chem. 103 (1993) 490–503.
[16] T. Atou, H. Faqir, M. Kikuchi, H. Chiba, Y. Syono, Mater. Res. Bull. 33 (2) (1998) 289–292.
[17] R.E. Dinnebier, S. Carlson, M. Hanfland, M. Jansen, Am. Mineral. 88 (2003) 996–1002.
[18] V.P. Itkin, C.B. Alcock, J. Phase Equil. 17 (6) (1996) 533–538.
[19] A. Grzechnik, L. Farina, R. Lauck, K. Syassen, I. Loa, P. Bouvier, J. Solid State Chem. 168 (2002) 184–191.
[20] J.D. McCullough, J. Am. Chem. Soc. 59 (1937) 789–794.
[21] K. Ståhl, J.P. Legros, J. Galy, Z. Krist. 202 (1992) 99–107.
[22] R. Shirley, The Crysfire 2002 System for Automatic Powder Indexing: User's Manual, The Lattice Press, 41 Guildford Park Avenue, Guildford, Surrey GU2 7NL, England, 2002.
[23] V.N. Makatun, V.V. Pechkovskii, Rus. J. Phys. Chem. 44 (10) (1970) 1522.
[24] H. Putz, J.C. Schön, M. Jansen, J. Appl. Cryst. 32 (1999) 864–870.
[25] Crystal Impact GbR, Endeavour 1.1, Internet: http://www.crystalimpact.com/endeavour, Email: infocrystalimpact.com, Bonn 2001.
[26] C. Larson, R.B. Von Dreele, General Structure Analysis System (GSAS), Los Alamos National Laboratory Report LAUR 86–748 (2000).
[27] J.-F. Bérar, P. Lenann, J. Appl. Cryst. 24 (1991) 1–5.
[28] K. Brandenburg, Diamond—Visual Crystal Structure Information System, Version 2.1d, 1997–2002 Crystal Impact GbR, http://www.crystalimpact.com.
[29] R. Hoppe, Z. Kristallogr. 150 (1979) 23–52.
[30] R. Hoppe, Angew. Chem. 82 (1970) 7–16;
Angew, Chem. Int. Ed. Engl. 9 (1970) 25–34.
[31] A. Anderson, W. Sanders, Smith, J. Raman Spectrosc. 31 (2000) 403–406.